

# Birefringence induced by irregular structure in photonic crystal fiber

In-Kag Hwang, Yong-Jae Lee, and Yong-Hee Lee

Department of Physics, Korea Advanced Institute of Science and Technology  
Daejeon 305-701, Korea  
[ikhwang@kaist.ac.kr](mailto:ikhwang@kaist.ac.kr)

**Abstract:** The unintentional birefringence induced by the irregular structure in photonic crystal fibers is analyzed numerically using the plane wave expansion method. The statistical correlations between the birefringence and the various irregularities are obtained. The birefringence is found to be largely dependent on the fiber design parameters as well as the degree of the irregularity. And the large pitch and the small air hole make the fiber less sensitive to the structural irregularity, which is successfully explained by the simple perturbation theory. The accuracy of our analyses is confirmed by the detailed investigation of computational errors. This study provides the essential information for the characterization and the design of low birefringence photonic crystal fibers.

©2003 Optical Society of America

**OCIS codes:** (060.2400) Fiber properties; (060.2280) Fiber design and fabrication; (260.1440) Birefringence; (260.5430) Polarization

---

## References and links

1. T. A. Birks, J. C. Knight, and P. St. J. Russell, "Endlessly single-mode photonic crystal fiber," *Opt. Lett.* **22**, 961-963 (1997).
2. J. C. Knight, J. Arriaga, T. A. Birks, A. Ortigosa-Blanch, W. J. Wadsworth, and P. St. J. Russell, "Anomalous dispersion in photonic crystal fiber," *IEEE Photon. Technol. Lett.* **12**, 807-809 (2000).
3. J. C. Knight, T. A. Birks, R. F. Cregan, P. St. J. Russell, and J. -P. de Sandro, "Large mode area photonic crystal fiber," *Electron. Lett.* **34**, 1347-1348 (1998).
4. A. Ortigosa-Blanch, J. C. Knight, W. J. Wadsworth, J. Arriaga, B. J. Mangan, T. A. Birks, and P. St. J. Russell, "Highly birefringent photonic crystal fibers," *Opt. Lett.* **25** 1325-1327 (2000).
5. Theis P. Hansen, Jes Broeng, Stig E. B. Libori, Erik Knudsen, Anders Bjarklev, Jacob Riis Jensen, and Harald Simonsen, "Highly birefringent index-guiding photonic crystal fibers," *IEEE Photon. Technol. Lett.* **13**, 588-590 (2001).
6. T. Niemi, H. Ludvigsen, F. Scholder, M. Legré, M. Wegmuller, N. Gisin, J. R. Jensen, A. Petersson, and P. M. W. Skovgaard, "Polarization properties of single-moded, large-mode area photonic crystal fibers," in *Proc. European Conference on Optical Communication 2002*, paper M.S1.09.
7. A. Peyrilloux, T. Chartier, A. Hideur, L. Berthelot, G. Mélin, S. Lempereur, D. Pagnoux, and P. Roy, "Theoretical and experimental study of the birefringence of a photonic crystal fiber," *J. Lightwave Technol.* **21**, 536-539 (2003).
8. M. J. Steel, T. P. White, C. Martijn de Sterke, and R. C. McPhedran, and L. C. Botten, "Symmetry and degeneracy in microstructured optical fibers," *Opt. Lett.* **26**, 488-490 (2001).
9. Se-Heon Kim and Yong-Hee Lee, "Symmetry Relations of Two-Dimensional Photonic Crystal Cavity Modes," *IEEE J. Quantum Electron.* **39**, 1081-1086 (2003)
10. S. B. Libori, J. Broeng, E. Knudsen, A. Bjarklev, and H. R. Simonsen, "High-birefringent photonic crystal fiber," in *Proc. Optical Fiber Communication Conference 2001*, Vol. 54 of OSA Proceedings Series (Optical Society of America, Washington, D.C., 1900), pp. TuM2-1 -TuM2-3.
11. S. G. Johnson and J. D. Joannopoulos, "Block-iterative frequency-domain methods for Maxwell's equations in a planewave basis," *Opt. Express* **8**, 173-190 (2001),  
<http://www.opticsexpress.org/abstract.cfm?URI=OPEX-8-3-173>
12. Yong-Jae Lee, Dae-Sung Song, Se-Heon Kim, Jun Huh, and Yong-Hee Lee, "Modal characteristics of photonic crystal fibers," *J. Opt. Soc. Korea* **7**, 47-52 (2003).
13. Masanori Koshiba, and Kunimasa Saitoh, "Numerical verification of degeneracy in hexagonal photonic crystal fibers," *IEEE Photon. Technol. Lett.* **13**, 1313-1315 (2001).
14. A. W. Snyder and J. D. Love, *Optical Waveguide Theory* (Chapman & Hall, New York, 1983), Chap. 18.

## 1. Introduction

The photonic crystal fibers (PCFs) have drawn great attention as the new waveguides with novel optical properties such as endlessly single mode operation [1], anomalous group velocity dispersion [2], and large effective core area [3]. Recently their polarization characteristics have been widely investigated. High birefringence PCFs preserving polarization states were successfully developed by introducing highly asymmetric fiber structures [4,5]. In symmetric PCFs, their birefringence and polarization mode dispersion were measured experimentally [6,7].

In many applications of PCFs, especially as an optical transmission medium for communication, it is important to suppress the birefringence to make the system polarization-insensitive. In the PCF with ideal symmetry, the two polarization modes are degenerate [8,9,13]. However, in real situation, maintaining the symmetry throughout the fiber fabrication processes is nontrivial, which results in the inevitable birefringence. The complicated structure of the PCF seems to make the PCF more susceptible to the unintentional birefringence than the conventional fiber.

For the characterization and the control of the birefringence in PCFs, it is critical to find the correlation between the birefringence and the irregularity of the fiber structure. Only a few studies have been done [10], and no thorough result is found in this area. In this paper, the birefringence of PCFs with various degrees of irregularity in various fiber designs is numerically analyzed and interpreted. Based on this study, the effective structure of the low birefringence PCF is also proposed.

## 2. Numerical birefringence of the perfect PCF

The structure of the photonic crystal fiber used in this study is shown in Fig 1. The index of silica is 1.45. This type of structure is specified usually by two parameters, the ratio of the air hole diameter to the pitch  $d/\Lambda$  and the scale factor  $\Lambda/\lambda$ . In this paper,  $d/\Lambda=0.48$  is selected for initial studies. It enables the single mode operation over a wide range of  $\Lambda/\lambda$ , at least between 1 and 11, and the relatively large hole size provides strong guidance of the optical mode against the fiber bend [1].

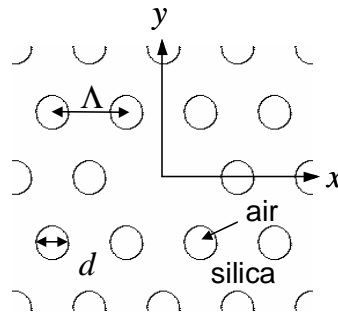


Fig. 1. Photonic crystal fiber structure.

The plane wave expansion method [11, 12] is used for the calculation of the birefringence throughout this paper. Since the birefringence we are dealing with is in the small range ( $\Delta n=10^{-4} \sim 10^{-7}$ ), it is important to guarantee the computation error to be below this level. The calculation accuracy in the plane wave expansion method is influenced by several parameters such as the number of plane waves, the size of the supercell, and the tolerance. The tolerance is the numerical criterion of zero to be reached through iterations. Here we try to find the optimum parameter set by repeating the calculation for the perfectly symmetric PCF while varying these computational parameters.

Figure 2 shows one of the variations: the mode index versus the spatial resolution. The spatial resolution is the number of grids per unit length  $\Lambda$ , and the total number of grids in the supercell is equal to the number of plane waves. As the resolution increases, the mode indices for two polarizations converge to one point which can be considered as the true value [13]. The modal birefringence, or the index difference between the two polarizations is plotted in Fig. 2 (b) at three different values of  $\Lambda/\lambda$ . This amount of numerical birefringence in the perfect PCF comes from the finiteness of the computational model, and limits the calculation accuracy of the actual birefringence. It should be noted that the numerical birefringence error is bigger at a longer wavelength ( $\lambda$ ) or for a smaller fiber structure ( $\Lambda$ ).

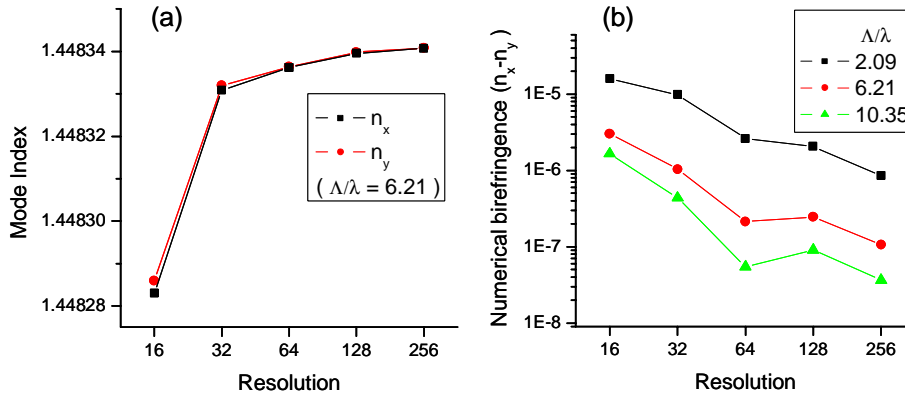


Fig. 2. (a) The mode indices for two polarizations versus grid resolution. (b) Numerical birefringence error versus grid resolution at various  $\Lambda/\lambda$ .

The size of supercell and the tolerance also affect the accuracy of the mode index in the fashion similar to that shown in Fig. 2(a). The optimum parameters are chosen based on the convergence of the mode indices and the computation time. The supercell size is chosen to be  $7\Lambda \times 7\Lambda$ , and the tolerance to be  $10^{-7}$ . In most calculations, the resolution of 64 is used, which corresponds to the number of plane waves of  $(7 \times 64)^2$ . Only when the total birefringence of a PCF sample is close to or below the numerical error level, that sample is recalculated with resolution of 256 to confirm the accuracy of the result.

Theoretically, in the structure with six-fold symmetry, the two polarization modes are degenerate [8,9]. However, with the finite spatial resolution used in our computation, the silica-air boundary is not perfectly circular, and thus the rotational symmetry of the whole structure is broken. If one increases the resolution, the holes become more circular and the symmetry is improved (although not perfect), which explains the behavior shown in Fig. 2. The numerical error increases as the hole diameter  $d/\Lambda$  decreases. However, the fluctuation of the error due to the variation of the hole size is still well below the real birefringence studied in this work.

The shape of the supercell as well as its size also affects the numerical error. Usually the supercell is defined as a rhombus, when describing the hexagonal lattice structure, with the shorter dimension in either  $x$  or  $y$ . When this supercell is resolved into the same number of grids along two sides of the rhombus, the grids have different densities (or resolutions) along  $x$ - and  $y$ -directions. The numerical error due to this uneven resolution also decreases with the dimension of the grid.

To verify the effect of the supercell shape, we try a different shape of the supercell which is a rectangle of  $7\Lambda \times 4\sqrt{3}\Lambda$ . In this case, the effective resolutions along  $x$  and  $y$  directions are different by only  $\sim 1\%$ . Figure 3 shows the calculated numerical birefringence at different resolutions. At the resolutions of 128 and 256, the numerical errors are much smaller than those shown in Fig. 2(b), which proves the effect of the supercell shape. In the following

calculations, however, the rhombus shape is used for the supercell, since no improvement is observed for the rectangular supercell at the resolution of 64.

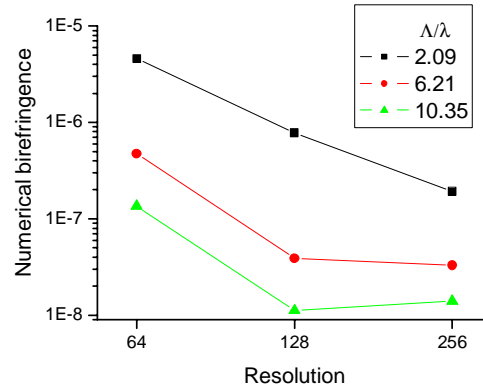


Fig. 3. Numerical birefringence error versus grid resolution at various  $\Lambda/\lambda$ , calculated with the rectangular supercell.

### 3. Birefringence of the PCFs with irregular structures

Since the irregularity means the partial ‘randomness’ of the structural parameters, only statistical analyses can be applied to correlate the birefringence with the irregularity. In the statistical analyses, the birefringence will be obtained as a probability distribution for a given degree of irregularity.

One major irregularity frequently found in the PCF is the variation of hole diameters. To simulate the practical situation, we assume that each hole diameter is given by the probability distribution of Gaussian as shown in Fig. 4(a). The mean value of the distribution is 0.46 and its standard deviation divided by the mean ( $\delta l/d$ ) serves as the degree of irregularity. First, with  $\delta l/d=0.2$ , 20 PCF samples are randomly generated and their birefringence are calculated using the above method. Figure 4(b) shows the birefringence distribution of the 20 samples at  $\Lambda/\lambda=6.21$ . Two insets show the fiber structures of two samples with the smallest and largest birefringence. The lower one has relatively uniform holes at the innermost ring, by accident, while the upper one shows the severe asymmetry. This confirms that the symmetry of innermost holes plays the major role for the birefringence of PCFs.

In this statistical model, the distribution of the birefringence cannot be expressed by a simple function form. There is non-zero probability of zero birefringence, and, at the same time, the maximum birefringence cannot be defined. The broad distribution suggests that the structural quality of PCFs can not be addressed by a few measurements of the birefringence [6]. From Fig. 4(b), the mean and the standard deviation are extracted to represent the birefringence distribution, which are  $5.0 \times 10^{-6}$  and  $3.0 \times 10^{-6}$ , respectively, in this case.

The same process is repeated for different values of  $\delta l/d$ , and the results are summarized in Fig. 4(c). The mean and the standard deviation of each distribution of the birefringence are plotted as dots and error bars, respectively. The data for  $\Lambda/\lambda = 6.21$  correspond to the birefringence, for example, at 1550 nm in a PCF with  $\Lambda=9.3 \mu\text{m}$  and  $d=4.3 \mu\text{m}$ . One interesting result is that the birefringence strongly depends on the scale factor  $\Lambda/\lambda$  [10]. Increasing the size of the fiber structure as well as suppressing the hole size variation will have significant effects on the reduction of the birefringence. The origin of this scale dependence will be discussed later.

The plot in Fig. 4 is useful for fiber fabricators who are concerned with the birefringence. For example, one can find that the hole size should be uniform within 2% to guarantee the birefringence below  $10^{-6}$ , at  $\Lambda/\lambda=6.21$ . Or, once they have knowledge about the structural quality of PCFs, their birefringence distribution can be estimated from the plot.

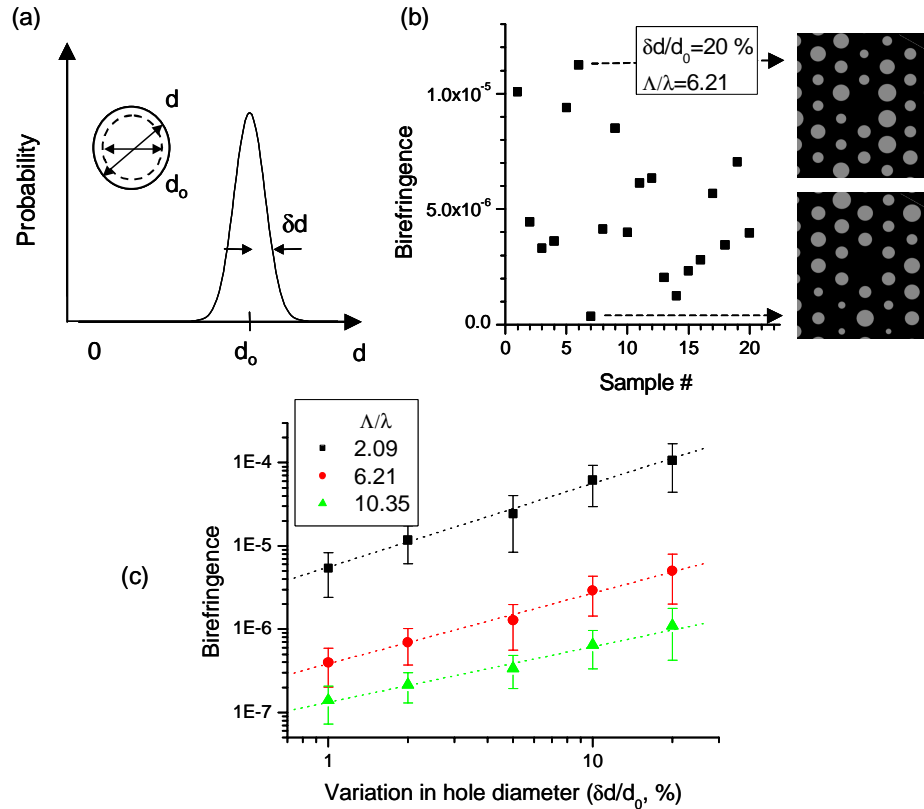


Fig. 4. Birefringence due to variation of hole diameters. (a) Probability distribution of each hole diameter,  $d$ :  $d_0$ , original hole diameter;  $\delta d$ , standard deviation of  $d$ . (b) Birefringence of 20 PCF samples with  $\delta d/d_0=0.2$ . Two insets are the structures of two PCFs with the largest and the smallest birefringence. (c) Birefringence of PCFs at various degrees of hole diameter variation. The marker and error bar denote the mean and the standard deviation, respectively, of birefringence distribution. The dotted lines are obtained by linear fitting of mean values.

Table 1. The fitting coefficients  $A$  and  $B$  of Eq. (1), obtained from the data in Fig. 4 (c)

$\Lambda/\lambda$	2.09	6.21	10.35
$A$	1.01	0.85	0.67
$B$	-5.25	-6.42	-6.88

When both the degree of the irregularity and the average birefringence are plotted in log scale as shown in Fig. 4(c), we can find a semi-empirical linear relation,

$$\log_{10}(\Delta n) = A \cdot \log_{10}\left(\frac{\delta d}{d} \cdot 100\right) + B \quad (1)$$

$$\Delta n = \left(\frac{\delta d}{d} \cdot 100\right)^A \cdot 10^B \quad (2)$$

where  $A$  and  $B$  are the fitting parameters. Table 1 shows  $A$  and  $B$  values at each scale factor.  $A$  is close to unity at the small value of  $\Lambda/\lambda$ , which means the magnitude of the birefringence is proportional to  $\delta d/d$  in Eq. (2). However, for large values of  $\Lambda/\lambda$ ,  $A$  is smaller than 1 and the birefringence grows slower than the linear case.

The second irregularity studied here is the displacement of the hole position. As shown in Fig. 5 (a), we assume the magnitude of the displacement,  $q$ , has the Gaussian probability distribution with a standard deviation,  $\delta q$ , and the direction of the displacement of each hole is random. The hole size is fixed at  $d/\Lambda=0.46$  and the degree of the hole position variation is defined as  $\delta q/\Lambda$ . 20 random samples are generated for each degree of the position variation. The mean and the standard deviation of the birefringence are plotted in Fig. 6. Again, the linear relation is found in the log-log plot, and its coefficients are shown in Table 2. The overall behaviors, including the dependence of the coefficient  $A$  on the scale factor, are found to be very similar between the two different types of the irregularities.

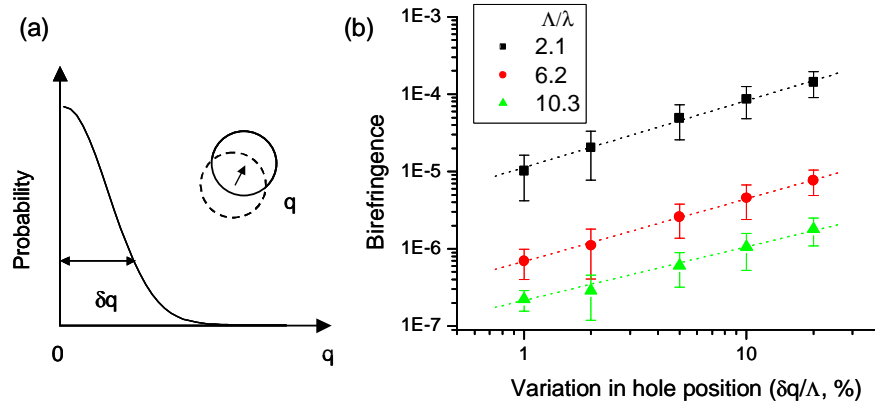


Fig. 5. Birefringence due to variation of hole positions. (a) Probability distribution of offset  $q$  in each hole:  $\delta q$ , standard deviation of  $q$ . (b) Birefringence of PCFs at various degrees of hole position variation. The marker and error bar denote the mean and the standard deviation, respectively, of birefringence distribution. The dotted lines were obtained by linear fitting of mean values.

Table 2. The fitting coefficients  $A$  and  $B$  of Eq. (1), obtained from the data in Fig. 5 (b)

$\Lambda/\lambda$	2.09	6.21	10.35
$A$	0.86	0.81	0.69
$B$	-4.95	-6.16	-6.67

The physical interpretation of the results in Fig. 4 and Fig. 5 can be given as follows. The structural irregularity, the variation of the hole size or the position results in the perturbation of the refractive index from the perfect structure. In the perturbed waveguide structure, the mode index change is proportional to the area of the perturbed region and the optical intensity in that region [14]. Since the birefringence is defined as the difference of the two mode indices, it is reasonable to argue that the birefringence is also dependent on the two factors although the dependency may not be exactly linear.

In the hole size variation, the perturbed area is given by the following equation.

$$S = \pi \left(\frac{d}{2}\right)^2 \quad (3)$$

$$\delta S_d \approx \frac{\pi}{2} d \cdot \delta d = \frac{\pi}{2} d^2 \cdot \left(\frac{\delta d}{d}\right) \quad (4)$$

where  $S$  is the hole area. In case of the hole position variation,

$$\delta S_q \approx 2d \cdot \delta q = 2d\Lambda \cdot \left( \frac{\delta q}{\Lambda} \right) \quad (5)$$

where  $\delta q$  is the offset from the original position. In both cases, the perturbed area  $\delta S$  is proportional to the degree of irregularity, in agreement with the semi-linear relations between the birefringence and  $(\delta d/d)$  or  $(\delta q/\Lambda)$ . The coefficient  $2d\Lambda$  in Eq. (5) is bigger than the coefficient  $(\pi/2)d^2$  in Eq. (4) by factor of  $\sim 2.8$ . It explains why the position-dependent birefringence is bigger than the size-dependent birefringence at the same degree of the irregularity. (Compare the  $B$  values in Table 1 and 2.)

The investigation of optical intensity distributions provides additional information. Figure 6 (a) shows the optical intensity profiles of a guided mode (y-polarized) as a function of  $x$  at  $y=0$  in Fig. 1. The vertical lines denote the boundary of innermost air holes, and the markers indicate the optical intensity at the first boundary. Note that the optical power is better confined in the silica for the larger structure or at the short wavelength, leaving little power in and around the holes. The intensity at the hole boundary for  $\Lambda/\lambda=2.09$  is more than 10 times stronger than that for  $\Lambda/\lambda=10.35$ . This observation is consistent with the suppression of the birefringence at the larger scale factor by factor of 30 ~ 100 as observed in Fig. 4(c) and 5(b).

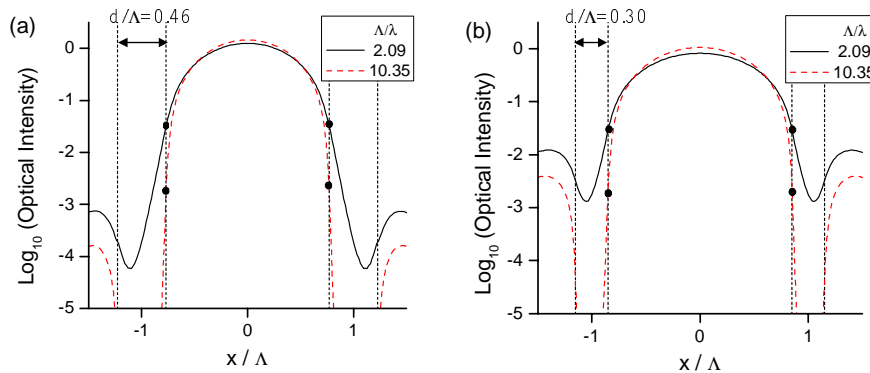


Fig. 6. Optical intensity profile as a function of  $x$  at  $y=0$ , for (a)  $d/\Lambda=0.46$  and (b)  $d/\Lambda=0.36$ . The dotted vertical lines denote the boundary of air holes. The solid and broken curves are intensity profiles for  $\Lambda/\lambda=2.09$  and  $10.35$ , respectively.

All the above analyses have been done for the specific hole size of  $d/\Lambda=0.46$ . To investigate the behavior at different hole sizes, the same process is repeated at  $d/\Lambda=0.30$  with the hole size variation of 10%. The obtained birefringence is lower than that shown in Fig. 4(c) for all  $\Lambda/\lambda$ , and it is equivalent to  $\sim 3\%$  hole size variation at  $d/\Lambda=0.46$ . This indicates that the PCF with the small holes is advantageous in suppressing the birefringence as long as  $\delta d/d$  is constant.

The optical intensity profile of the small hole PCF is shown in Fig. 6(b). The intensity at the first hole boundary is almost the same as that of the large-hole PCF shown in (a). However, the area of the perturbed region is calculated differently in Eq. (4) since it is proportional to  $d^2$ . The reduction of the hole diameter from 0.46 to 0.30 results in the reduction of  $dS_d$  by factor of 2.4, which explains the reduction of the birefringence.

#### 4. Design for low birefringence fibers

As found in the above analyses, the PCF with a large scale factor  $\Lambda/\lambda$  and/or a small hole size  $d/\Lambda$  is desirable for the lower birefringence assuming the degrees of the regularities  $(\delta d/d)$  and  $(\delta q/\Lambda)$  are determined regardless of  $d$  and  $\Lambda$ . Especially, increasing the scale factor is very

effective. For example, the increase of the scale factor by a factor of 2 brings the equivalent effect of reducing the degree of regularity by a factor of  $\sim 10$ . (See Fig. 4(c) and 5(b).)

However, the design toward the low birefringence may sacrifice other important fiber characteristics such as the number of guided modes, the mode size, and the bend loss. The larger scale factor and the smaller hole size do not increase the number of guided modes, fortunately. The mode size is not much different from the core size,  $(2\Lambda-d)$ , so it is approximately proportional to the scale factor. The bend loss, in general, depends on the effect index difference between the core and the cladding regions, which decreases at the larger scale factor and the smaller hole size, resulting in the higher bend losses [1].

Therefore, to minimize the birefringence of PCFs at a given wavelength  $\lambda$ , it is desirable to maximize the pitch  $\Lambda$ , and minimize the hole size  $d$  as long as the mode size and the bend loss allow.

Another factor that affects the birefringence of the PCF, other than the structural irregularity, could be the stress. The stress in the PCF has not been yet investigated in detail. However, the stress field must be closely related to the physical structure. For example, the perfect structure would have the symmetric stress field resulting in zero-birefringence. The stress effect will most likely amplify or diminish the geometrical birefringence, instead of acting as an independent birefringence source.

## 5. Conclusion

The birefringence due to the structural irregularity in the PCF is extensively investigated by numerical analyses. The statistical correlations between the birefringence and the degree of the irregularity are obtained, and their behaviors are explained by the simple perturbation theory. It is found that the birefringence can be effectively suppressed in the PCFs with the large pitch and the small hole. The numerical errors in the plane wave expansion method are investigated in detail to find their origins and confirm the accuracy of our analyses. The information obtained in this study can be utilized in the characterization and the estimation of the birefringence in PCFs, and also in the design of the low birefringence PCF.

## Acknowledgments

This work was supported by the National Research Laboratory Project of Korea, and the National R&D Project for Nano Science and Technology.